Long-period fiber grating sensor interrogation with single strain modulated FBG and harmonic analysis

Guilherme Sampaio, Felipe Oliveira Barino, and Alexandre Bessa dos Santos

***Abstract*— Optical fiber sensors have been used in diverse applications due to their intrinsic characteristics. A widely used, partly due to its interaction with many different external parameters, is the long-period fiber grating sensor (LPFG). The challenge in using LPFGs lies in their interrogation technique, which relates the change in optical characteristics with the measurand. This paper presents a method for the interrogation of LPFG sensors. The method uses a single FBG attached to a vibrating piezoelectric component and analyses the harmonic components of the optical power reflected by the FBG. The method was tested via simulations on several arc-induced LPFGs spectra and achieved results comparable to an established method for half of the test set and improved by roughly 5 times the resonant wavelength accuracy and precision by limiting the dynamic range.**

***keywords*— fiber optical sensors, long-period fiber grating, interrogation technique, fiber Bragg grating, harmonic analysis**

I. Introduction

Long-period fiber grating sensors have been used in diverse applications, from structural health monitoring to biochemical detection [1]–[3]. This widespread use could be credited to their intrinsic characteristics, such as electromagnetic interference immunity, high sensitivity, and low attenuation. Additionally, they are small, lightweight, resistant to chemicals, do not require any electric current [4], and are widely applicable. A great variety of applications for LPFG sensors can be explained by the variety of physical quantities that interact with them: temperature [5], deformation [6], and surrounding refractive index [7].

LPFG sensors are based on optical fiber gratings, thus manufactured through periodic modulation of the optical fiber properties, such as refractive index [8] or geometry [9], for example. Fiber diffraction gratings are devices that promote mode coupling. A LPFG couples light from the fiber's fundamental guided core mode into co-propagating cladding modes. The energy coupled to the cladding mode is then attenuated due to scattering of light at the medium interface, resulting in a band-stop transmission characteristic centered at the wavelength in which mode coupling occurs.

Moreover, in a single mode fiber, the fiber cladding is larger than the core (125 µm and 8.2 µm diameter, respectively, for a SMF-28), thus allowing the existence of several possible modes. Therefore, the transmission spectrum of an LPFG could have several stop bands with unique sensitivities [10]. Consequently, more information can be gathered from a single LPFG sensor, allowing the rise of multi-measurement and self-compensating single-LPFG sensing schemes [11]–[16].

The challenge in using LPFGs lies in their interrogation technique, which relates the change in optical characteristics with the measurand. The main challenge is the large FWHM of LPFGs [17]. The interrogation of LPFGs is often related to the measurement of the resonance wavelength of the transmission spectrum and a way of doing so directly is through the use of a broadband light source to illuminate the LPFG and an optical spectrum analyzer (OSA) to measure the spectrum. This method is precise and works with different LPFGs, which makes it suitable for LPFG production labs, for example. However, the OSA has several disadvantages such as high weight, volume, cost, and power consumption, which renders them incompatible for in-field use.

Another approach is to use two fiber Bragg grating (FBGs) filters with optimized Bragg wavelengths to match the edges of a LPFG stopband [18]. The reflection of each FBG is read in terms of the optical power filtered by them. The use of two FBGs relates to the linearization of the calibration curve using a single parameter (R), calculated from both optical powers (P_{FBG_1} and P_{FBG_2}) through the equation:

$$R = \frac{P_{FBG_1} - P_{FBG_2}}{P_{FBG_1} + P_{FBG_2}} \quad (1)$$

Note that the parameter R is then used as the input for an unidimensional linear regression with the measured quantity value (y) as the output ($y = f(R) = a \cdot R + b$) during the sensor calibration.

In this paper, a method based on the latter (which is our baseline and will be referred to as the traditional method) is proposed. The proposed method was based on a single FBG modulated by a lead zirconate titanate piezoelectric transducer (PZT). The modulated filter was used to acquire a time-varying electrical signal by means of a photodetector module. This module consisted of a NIR photodiode coupled to a transimpedance amplified and an analog-digital converter. The converted signal was then analyzed in the frequency domain to retrieve the LPFG sensor central wavelength.

Our proposal reduces the need for the two FBGs used in the traditional method and eases the interrogation of multiple LPFGs. Note that the same processing circuit could be used for several LPFG sensors, if needed. To do so, a PZT per LPFG should be used and each PZT should be modulated with a single frequency. Therefore, the LPFG information that is

retrieved by the FBG filter is frequency multiplexed.

There is a need for cost effective interrogation models for fiber sensors, and one notable approach was proposed in [19], which suggests the use of catastrophic fuse effect micro-cavity interferometers for FBG interrogation. Some similar LPFG interrogation methods have been proposed, however they use the two modulated FBGs and focus on performance increase instead of cost reduction [20]. One work has proposed a more similar approach, concerning the optical setup, using a single FBG modulated by a PZT [21]. However, the proposed method focused on rebuilding the resonant valley, approximating it to a Gaussian curve. Bernardo et al proposed a low-cost system for the interrogation also based on the reconstruction of the optical spectrum, using thermally modulated distributed feedback lasers to sweep a narrow band of the optical spectrum in [22]. Thus, our work presents a simpler and fully data driven model that could be easily fitted during the LPFGs sensor calibration and targets the extraction of the resonant wavelength. We also present an evaluation of the proposed interrogator using several LPFGs, thus investigating the generalization capability of our approach.

II. Setup and Methods

A. Theoretical concepts for LPFGs and FBGs

As previously discussed, LPFGs are in-fiber diffraction gratings with band-stop transmission characteristic, induced by the mode coupling. The wavelength in which the core mode is coupled to a m^{th} cladding mode is called a resonant wavelength and is given by [8]:

$$\lambda_{res}^{m} = \left(n_{eff,co} - n_{eff,cl}^{m}\right)\Lambda \qquad (2)$$

where Λ is the grating modulation period, $n_{eff,co}$ and $n_{eff,cl}^{m}$ are, respectively, the effective refractive index of core and m^{th} cladding modes. Note that Λ changes with mechanical deformation and thermal expansion; whereas $n_{eff,co}$ and $n_{eff,cl}^{m}$ change with photo-elastic and thermos-optic effects; additionally, $n_{eff,cl}^{m}$ depends on the surrounding refractive index. These dependencies justify the use of LPFGs as sensing devices and the wide use of the resonant wavelength λ_{res}^{m} as the measurand-encoding parameter for the calibration of an LPFG sensor.

FBGs are also in-fiber grating devices, but such devices reflect the coupled light. The short period of FBGs promotes coupling from the fundamental core mode to a counter-propagating core mode, thus reflecting light at the wavelength in which the coupling occurred. Therefore, FBGs could be used as a selective mirror; namely a pass-band optical filter, considering its reflection transfer characteristic. Considering its transmission transfer characteristic FBGs are also band-stop filters, but with much smaller FWHM. For FBGs, the wavelength in which coupling occurred is called Bragg wavelength and is given by [8]:

$$\lambda_{Bragg} = 2n_{eff,co}\Lambda \qquad (3)$$

Note that, similarly to LPFGs, FBGs are also sensitive to strain and temperature [23], [24].

B. LPFG data and FBGs positioning

We a tested our proposal for 14 arc-induced LPFGs manufactured with $\Lambda = 430\ \mu$m. Each LPFG was illuminated using a broadband light source and subjected to five different strain values in order to stimulate a resonant wavelength shift; the spectrum for each case was recorded using an OSA. Thus our database was comprised of 14 groups of five LPFG spectra, summing 70 LPFG spectra in total. The spectra were collected and preprocessed to compensate the light source, therefore obtaining the 70 transmission transfer functions. These transmission characteristic were processed to extract each resonant wavelength, and then the proposed interrogator was simulated and analyzed. Fig. 1 shows the transmission spectra of the 14 LPFGs resting at room temperature.

It was expected that choosing the FBG position for each individual LPFG would increase the overall performance of the interrogator. This would, however, also mask the generalization capability of the proposed interrogator. Thus, for the entire study, one single FBG resonant wavelength was chosen for the proposed method. This filter was designed to stay around the mean resonant wavelength of our LPFG spectra database, namely 1.5424 μm. For comparison, two FBGs were also chosen to simulate the traditional method. These were designed to have a slightly lower Bragg wavelength than the lowest expected LPFG resonant wavelength, and the other slightly higher than the highest LPFG resonant wavelength. The values were 1.537 μm and 1.547 μm. All FBGs had FWHM of ~1 nm.

The extreme LPFGs spectra alongside the FBGs reflection

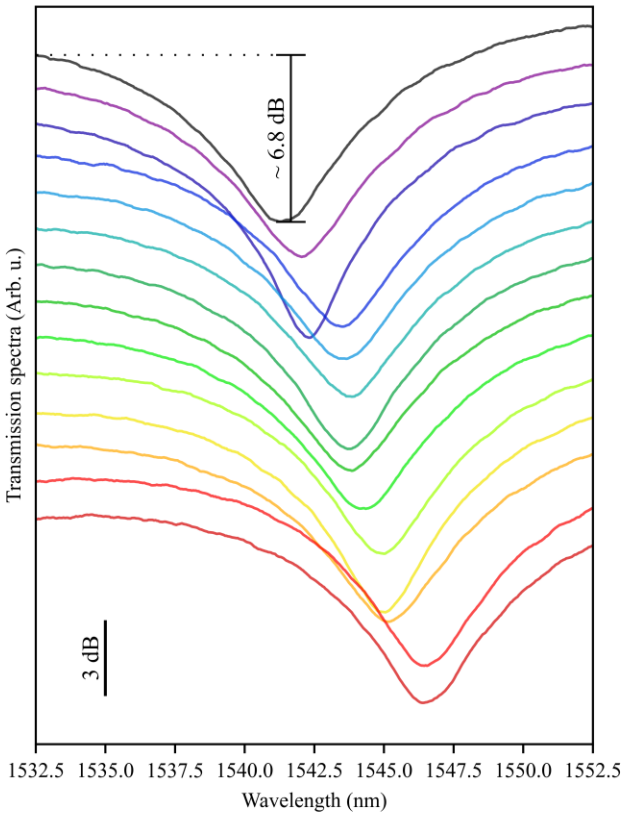

Fig. 1. Spectra of the 14 LPFGs used to test the proposed interrogation method.

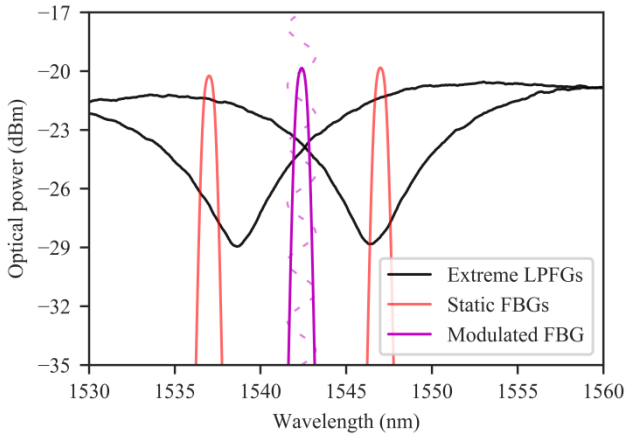

Fig. 2. Spectra of the extreme resonant wavelength LPFGs and FBG filters. Dotted line represents the FBG modulation.

spectra can be seen in Fig. 2, so the range of all 70 spectra could be better visualized. Therefore, in this figure one can see the interrogator resonant wavelength dynamic range, the spectral characteristic of the FBG used to filter the LPFGs, and the spectra of the FBG pair used for the traditional method as baseline.

C. *Interrogation setup*

The setup for the proposed interrogator is schematized in Fig. 3 and it was simulated in python using the LPFG data base as input. The FBG spectrum was simulated following the approximated equation presented in [25]. The FBG modulation was simulated according to the values presented in [26]: an FBG attached to a PZT, which was connected to an AC voltage of 127 V @ 60 Hz, with a Bragg wavelength shift of 6.475 pm/V. The light source considered was a S5FC1550S-A2 from ThorLabs.

The setup was simulated based on each device transfer function, the input light was filtered by the LPFG and later had a part reflected by the FBG towards the photodetector. The time varying simulation was taken in order to simulate a generic microcontroller collecting the photodetected signal at a sampling rate (f_s) related to the maximum harmonic order (n) collected at the test and to the PZT frequency (f_{PZT}).

$$f_s = 2nf_{PZT} \qquad (3)$$

Fig. 4 illustrates the simulation and an acquired signal. In this figure, one can see an LPFG spectrum at the center. The modulated FBG filters this spectrum with a Bragg wavelength which varies accordingly to the dotted sinusoid. The dashed line represents the central Bragg wavelength. The photodetected signal is shown on the right side, as well as its DFT amplitude.

D. *Data processing*

The full circuit was simulated based on the acquired LPFG spectra and the simulated setup discussed in the previous subsection III-C. The harmonics were calculated with the fast Fourier transform (fft) algorithm up to the 1st and then up to the 2nd order, in two different tests. These values, along with the already detected LPFG resonant wavelengths were then stored for later analysis.

Additionally, simulations were also made using two static

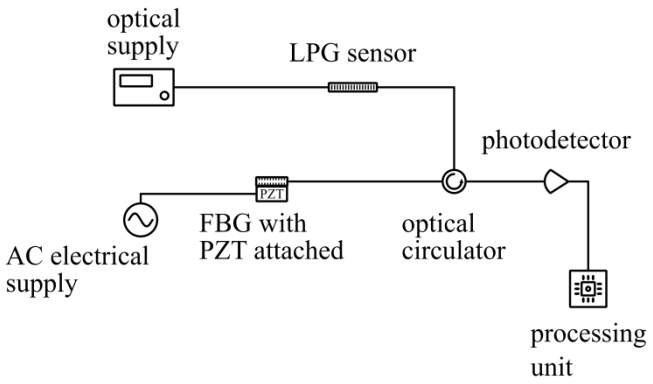

Fig. 3. Scheme of the proposed interrogation method.

FBGs (baseline interrogator) following the method described in the introduction, so that the comparison could be made easier. The LPFGs and the FBGs can be seen in the Fig. 2.

Then, for each unique LPFG, a linear regression through the linear least squares method, considering the resonant wavelength as output, was performed for both the traditional and proposed method. For the traditional method, the linear regression was unidimensional ($y = ax + b$), and used the R value calculated by eq. (1).

For the proposed method, $R^2 \rightarrow R$ and $R^3 \rightarrow R$ regression models were used, the first with two harmonics (harmonics of order 0 and 1) and the latter with three harmonics (harmonics of order 0, 1, and 2), respectively. For those, the inputs were the magnitude of the harmonic components. Let x_i be the i-th input, representing the i-th harmonic, the mathematical models were:

$$\hat{\lambda}_{res} = a_0 x_0 + a_1 x_1 + b \qquad (4)$$

for the two component model and

$$\hat{\lambda}_{res} = a_0 x_0 + a_1 x_1 + a_2 x_2 + b \qquad (5)$$

for the three component model.

To compare the methods three metrics were used: coefficient of determination (R^2), mean absolute error (MAE), and root mean square error (RMSE). MAE is the mean of the absolute errors for each data entry for the test set, lower is better. RMSE is the square root of the mean of the squared errors for each data entry in the test set. It also helps to visualize errors, but, unlike MAE, it punishes higher errors. In

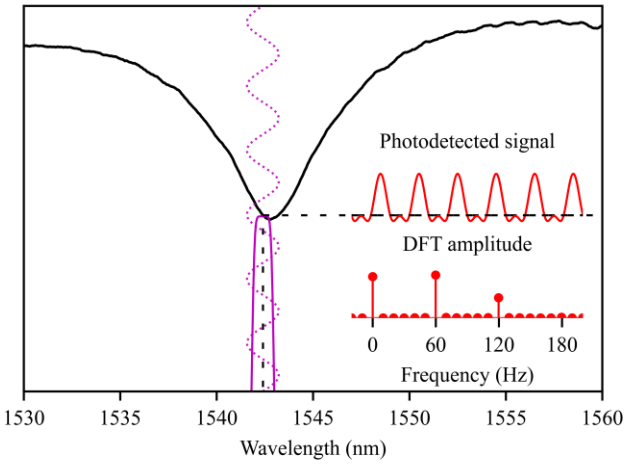

Fig. 4. Photodetected signal as a function of the FBG modulation.

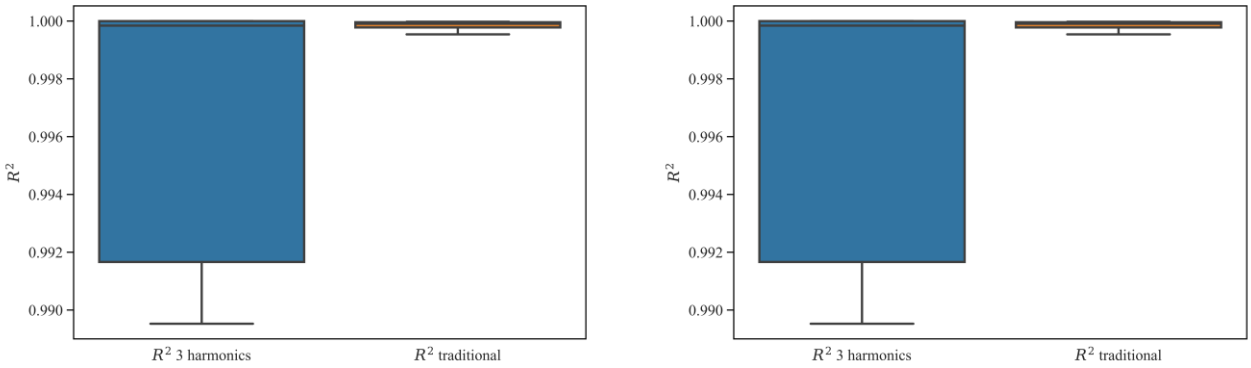

Fig. 5. Metrics distribution box plot for the 3 harmonics proposed and the traditional baseline method. (a) Errors: mean absolute error (MAE) and root mean squared error (RMSE). (b) R^2

general, the MAE is related to the accuracy, while the RMSE is related to the precision.

III. Results and Discussions

As aforementioned, the proposed method was tested against the traditional method. The distribution of the calculated metrics from the simulations for both methods can be found on Fig. 5. The metrics for the method with only two harmonics were abysmal. The mean R^2 was 0.6765, with a standard deviation of 0.4079, and the errors were about ten times higher than the errors for the method with three harmonics. Plotting these metrics along with the others would make the analysis harder, since the graphs would need to have higher limits, thus lower precision. As such, they were omitted. Inspecting the box plots, we could see that when using harmonics up to the second order, the results reached reasonable values. Although the minimum R^2 was 0.9894, low compared to the minimum of 0.9995 for the traditional method, the proposed method reached an R^2 of 0.9998 at the median, against 0.9999. This means a comparable result for 50% of the LPFGs. It should be noted that some points had a lower R^2 value. These points, however, were considered to be outliers, through the method of inter-quartile range (IQR).

As for the errors, a similar pattern to the one observed for the R^2 could be seen: The error was very high and varied wildly for the first test, but got considerably better when using the three calculated harmonic amplitudes. As such, the error analysis was done considering only the latter. Looking at the mean absolute errors (MAE) for both methods, it could be seen that the proposed was less reliable, it reached a maximum of 271 pm, against 21.9 pm, a little over 10 times worse. We only got comparable values when reaching the median, where it was 9.94 pm for the proposed method against 8.64 pm for the traditional.

It could also be seen that the RMSE was very close to the MAE for the proposed method, which means that there is not a great variance in the errors absolute values.

It is interesting to note that, as the simulation only takes into consideration the magnitude of the harmonic components, readings from spectra with their resonant wavelength higher than the FBG resonant peak will be very similar to readings from spectra with their resonant wavelength lower than the FBG resonant peak by a similar value. That could cause poor calibration for the LPFGs where sometimes the spectra had the left side of the resonant dip filtered by FBG, and other times the right side was filtered. To check that, the individual approximation error, for each spectrum, was plotted in Fig. 6. The LPFG types were color-coded to represent the difference mentioned: The points in yellow come from single edged LPFGs and the blue points from double edged LPFGs. For single edged LPFGs the resonant wavelength was either greater or smaller than the filter Bragg wavelength, thus only one edge of the resonant dip was filtered by the FBG. On the other hand, double edged LPFGs had both edges filtered. The x-axis is represented in difference between the spectra resonant and the FBG resonant wavelength (without modulation). Also, each symbol represents one unique LPFG, note that the yellow symbols representing the single edged LPFGs don't cross the $x = 0$ nm. It could be seen that the interrogation method performance was drastically higher for those single edged LPFGs, confirming what was mentioned at the beginning of the paragraph.

In fact, for the single edged LPFGs subset, the MAEs had a mean of 1.75 pm, with a minimum of 0.0897 pm and a maximum of 5.62 pm. This would make this method consistently better than the traditional method at the cost of a

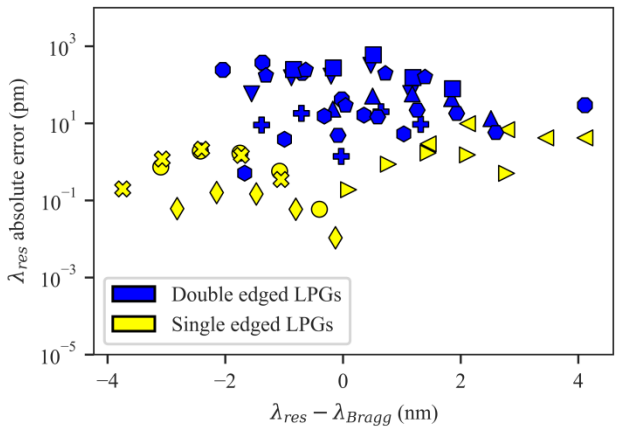

Fig. 6. Individual errors. Each symbol represents a single LPFG.

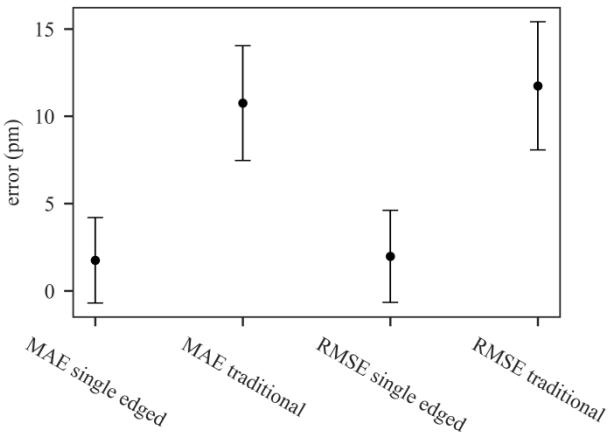

Fig. 7. Comparison metrics between the single edged group and the baseline.

dynamic range reduction. Note that restricting the LPFG resonant wavelength to operate at the single edge regime; the interrogation setup reduces the dynamic range roughly by half. Indeed, at the single edge regime, the LPFG resonant wavelength should lie either at the [1.537, 1.5424] μm interval or at the [1.5424, 1.547] μm. For the baseline method, on the other hand, the detectable interval is [1.537, 1.547] μm. But the detection limit reduction might be beneficial.

To illustrate the advantage of the proposed method over the baseline, i.e. the traditional method, the MAE and RMSE of both approaches are summarized in Fig. 7. This plot shows the mean value for each metric over the single edged subset of the proposed method and for the baseline, the error bars represent the 95% confidence interval of the mean. The results showed the proposed method potential for the single edged case, with accuracy and precision improvements, compared to the baseline method. The single edged metrics were ~5 times smaller than the traditional method metrics. Thereof, despite the dynamic range reduction, the precision and accuracy concerning the full scale was still improved.

During our simulations, the LPFGs were considered static and the resonant wavelengths estimated by curve fitting were considered ground-truth. Therefore the errors and uncertainties discussed in this work are concerning the proposed interrogation method alone. Furthermore, the proposed interrogator could be used for any LPFG sensor, thus for any measurand. Hence, the uncertainty characterized in this work is part of the sensor's combined uncertainty and could be used to express the measurement uncertainty, as described in [27].

IV. Conclusion

The interrogation of the LPFG sensors was achieved by using a single FBG attached to a PZT and calculating the harmonic components of the reflected optical power. The proposed method reached similar performances to an already consolidated interrogation method for half of the tests. For the other half, the error was about 10 times higher (calculated comparing the maximums and third quartiles). It is also important to note that the higher errors were concentrated on the double edged FBG. The results indicate the errors for single edged LPFGs were (~5 times) better than the errors for the traditional method.

The method might be viable in applications that require less precision over a wide dynamic range, or that require good precision over a reduced λ_{res} range. The results found on the single edged LPFGs showed a great potential for the proposed method. We believe the single edged LPFGs presented better results due to ambiguous harmonic amplitude information when the resonant dip passes the modulated FBG mean value. Therefore, on future works it is suggested to take the principal harmonic phase into consideration. Note that, when the resonant dip passes the modulated FBG mean, a 180° shift at the photodetector signal should be observed, due to the change in the LPFG slope.

To further improve upon this work, more studies could be done, such as using the harmonics phase information, using the method with more harmonics, and exploring different regression methods. Also, to further test the method's generalization capability, it could be used to interrogate more disperse LPFGs. Additionally, the same study could be run on a real setup, since simulations might not capture perfectly all the random changes and errors that occur on real life systems.

Acknowledgements

This work was supported in part by the Coordenação de Aperfeiçoamento Pessoal de Nível Superior (CAPES), Conselho Nacional de Desenvolvimento Científico e Tecnológico (CNPq), Fundação de Amparo à Pesquisa do Estado de Minas Gerais (FAPEMIG), Instituto Nacional de Energia Elétrica (INERGE-UFJF), and Ambev.

References

[1] Y. Huang, F. Tang, X. Liang, G. Chen, H. Xiao, and F. Azarmi, "Steel bar corrosion monitoring with long-period fiber grating sensors coated with nano iron/silica particles and polyurethane," *Struct. Heal. Monit. An Int. J.*, vol. 14, no. 2, pp. 178–189, Mar. 2015, doi: 10.1177/1475921714560070.

[2] B. Xu, J. Huang, L. Ding, and J. Cai, "Graphene oxide-functionalized long period fiber grating for ultrafast label-free glucose biosensor," *Mater. Sci. Eng. C*, vol. 107, p. 110329, Feb. 2020, doi: 10.1016/j.msec.2019.110329.

[3] F. Esposito *et al.*, "Long period grating in double cladding fiber coated with graphene oxide as high-performance optical platform for biosensing," *Biosens. Bioelectron.*, vol. 172, p. 112747, Jan. 2021, doi: 10.1016/j.bios.2020.112747.

[4] F. Chiavaioli *et al.*, "Femtomolar Detection by Nanocoated Fiber Label-Free Biosensors," *ACS Sensors*, vol. 3, no. 5, pp. 936–943, May 2018, doi: 10.1021/acssensors.7b00918.

[5] J. Hromadka *et al.*, "Simultaneous in situ temperature and relative humidity monitoring in mechanical ventilators using an array of functionalised optical fibre long period grating sensors," *Sensors Actuators B Chem.*, vol. 286, pp. 306–314, May 2019, doi: 10.1016/j.snb.2019.01.124.

[6] K. Kalli *et al.*, "Sensing properties of femtosecond laser-inscribed long period gratings in photonic crystal fiber," *Photonic Sensors*, vol. 1, no. 3, pp. 228–233,

Sep. 2011, doi: 10.1007/s13320-011-0013-8.

[7] K. R. Cooper, J. Elster, M. Jones, and R. G. Kelly, "Optical fiber-based corrosion sensor systems for health monitoring of aging aircraft," in *2001 IEEE Autotestcon Proceedings. IEEE Systems Readiness Technology Conference. (Cat. No.01CH37237)*, pp. 847–856, doi: 10.1109/AUTEST.2001.949466.

[8] T. Erdogan, "Fiber grating spectra," *J. Light. Technol.*, vol. 15, no. 8, pp. 1277–1294, 1997.

[9] I. Navruz, F. Ari, M. Bilsel, and Z. A. AL-Mashhadani, "Enhancing refractive index sensitivity using micro-tapered long-period fiber grating inscribed in biconical tapered fiber," *Opt. Fiber Technol.*, vol. 45, pp. 201–207, 2018, doi: https://doi.org/10.1016/j.yofte.2018.07.018.

[10] V. Bhatia and A. M. Vengsarkar, "Optical fiber long-period grating sensors," *Opt. Lett.*, vol. 21, no. 9, p. 692, May 1996, doi: 10.1364/OL.21.000692.

[11] F. S. Delgado and A. B. dos Santos, "Multi-measurement scheme for a fiber-optic sensor based on a single long-period grating," *J. Mod. Opt.*, vol. 64, no. 21, pp. 2428–2432, Nov. 2017, doi: 10.1080/09500340.2017.1367854.

[12] J. Hromadka *et al.*, "Multi-parameter measurements using optical fibre long period gratings for indoor air quality monitoring," *Sensors Actuators B Chem.*, vol. 244, pp. 217–225, 2017.

[13] C. Trono, F. Baldini, M. Brenci, F. Chiavaioli, and M. Mugnaini, "Flow cell for strain- and temperature-compensated refractive index measurements by means of cascaded optical fibre long period and Bragg gratings," *Meas. Sci. Technol.*, 2011, doi: 10.1088/0957-0233/22/7/075204.

[14] Y.-P. Wang, L. Xiao, D. N. Wang, and W. Jin, "Highly sensitive long-period fiber-grating strain sensor with low temperature sensitivity," *Opt. Lett.*, 2006, doi: 10.1364/ol.31.003414.

[15] Q. Ling, Z. Gu, W. Wu, and B. Pang, "Simultaneous SRI and temperature measurement of FM-LPFG written by CO2 laser," *Opt. Fiber Technol.*, vol. 58, p. 102264, Sep. 2020, doi: 10.1016/j.yofte.2020.102264.

[16] M. Chen, Y. Zhao, H. Wei, and S. Krishnaswamy, "Cascaded FPI/LPFG interferometer for high-precision simultaneous measurement of strain and temperature," *Opt. Fiber Technol.*, vol. 53, p. 102025, Dec. 2019, doi: 10.1016/j.yofte.2019.102025.

[17] F. O. Barino and A. B. dos Santos, "LPG Interrogator Based on FBG Array and Artificial Neural Network," *IEEE Sens. J.*, vol. 20, no. 23, pp. 14187–14194, Dec. 2020, doi: 10.1109/JSEN.2020.3007957.

[18] H. J. Patrick, G. M. Williams, A. D. Kersey, J. R. Pedrazzani, and A. M. Vengsarkar, "Hybrid fiber Bragg grating/long period fiber grating sensor for strain/temperature discrimination," *IEEE Photonics Technol. Lett.*, vol. 8, no. 9, pp. 1223–1225, Sep. 1996, doi: 10.1109/68.531843.

[19] C. A. R. Díaz *et al.*, "A cost-effective edge-filter based FBG interrogator using catastrophic fuse effect micro-cavity interferometers," *Measurement*, vol. 124, pp. 486–493, Aug. 2018, doi: 10.1016/j.measurement.2018.03.067.

[20] J. P. Carvalho *et al.*, "Long-Period Gratings Dynamic Interrogation With Modulated Fiber Bragg Gratings and Optical Amplification," *IEEE Sens. J.*, vol. 12, no. 1, pp. 179–183, Jan. 2012, doi: 10.1109/JSEN.2011.2128305.

[21] P. X. Neto, A. C. Carneiro, A. P. López-Barbero, V. N. H. Silva, R. M. Ribeiro, and A. B. dos Santos, "A Mathematical Model for the Interrogation of LPG Fiber Optical Sensors Based on Electrical Harmonic Analysis," *IEEE Sens. J.*, vol. 20, no. 8, pp. 4237–4244, 2020, doi: 10.1109/JSEN.2019.2963275.

[22] B. Dias, P. Santos, P. A. S. Jorge, J. M. M. M. de Almeida, and L. C. C. Coelho, "Spectral Reconstruction and Bayesian Model Framework for Characterization of Long Period Fiber Gratings," *IEEE Instrum. Meas. Mag.*, vol. 24, no. 5, pp. 56–62, Aug. 2021, doi: 10.1109/MIM.2021.9491007.

[23] L. Fang, T. Chen, R. Li, and S. Liu, "Application of embedded fiber Bragg grating (FBG) sensors in monitoring health to 3D printing structures," *IEEE Sens. J.*, vol. 16, no. 17, pp. 6604–6610, 2016.

[24] L. Jin *et al.*, "An embedded FBG sensor for simultaneous measurement of stress and temperature," *IEEE Photonics Technol. Lett.*, vol. 18, no. 1, pp. 154–156, Jan. 2006, doi: 10.1109/LPT.2005.860046.

[25] F. G. Peternella, B. Ouyang, R. Horsten, M. Haverdings, P. Kat, and J. Caro, "Interrogation of a ring-resonator ultrasound sensor using a fiber Mach-Zehnder interferometer," *Opt. Express*, vol. 25, no. 25, pp. 31622–31639, 2017.

[26] A. Dante, R. M. Bacurau, A. W. Spengler, E. C. Ferreira, and J. A. S. Dias, "A Temperature-Independent Interrogation Technique for FBG Sensors Using Monolithic Multilayer Piezoelectric Actuators," *IEEE Trans. Instrum. Meas.*, vol. 65, no. 11, pp. 2476–2484, Nov. 2016, doi: 10.1109/TIM.2016.2594021.

[27] G. R. C. Possetti, R. C. Kamikawachi, M. Muller, and J. L. Fabris, "Metrological Evaluation of Optical Fiber Grating-Based Sensors: An Approach Towards the Standardization," *J. Light. Technol.*, vol. 30, no. 8, pp. 1042–1052, Apr. 2012, doi: 10.1109/JLT.2011.2167500.